Flat-face epoxy-bonded concrete joints loaded in torsion

Chernin, Leon; Newlands, Moray; Khosravi, Noushin

Published in:
Construction and Building Materials

DOI:
10.1016/j.conbuildmat.2023.134558

Publication date:
2024

Construction and Building Materials 411 (2024) 134558

Contents lists available at ScienceDirect

Construction and Building Materials

journal homepage: www.elsevier.com/locate/conbuildmat

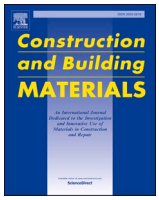

Flat-face epoxy-bonded concrete joints loaded in torsion: Physical modelling

Leon Chernin *, Moray Newlands, Noushin Khosravi

School of Science and Engineering, University of Dundee, DD1 4HN, UK

ARTICLE INFO

Keywords:
Epoxy
Concrete joint
Torsion
Shear
Experimental study
Digital Image Correlation

ABSTRACT

Joints in concrete structures must perform under various complex loads including torsion. This paper reports the results of an experimental programme investigating the static torsional performance of epoxy-bonded concrete joints. Torsion tests were performed using a custom experimental setup able to apply torque on a hollow concrete prism with an epoxy joint in the middle. The tested specimens failed in both cohesive and mixed modes. The cohesive failure mode was characterised by cracking in the body of concrete, while the mixed mode also included partial debonding of the joint. The cohesive mode was dominant, more ductile and exhibited higher torsional strength. The cracking behaviour of the jointed specimens was typical of concrete prisms under torsion except that in the mixed mode a crack developed along the joint on two or three specimen sides. Digital Image Correlation, applied for monitoring surface strain, showed that inclined bands of high shear strain passed across the joint during the tests. The mechanism of concrete-epoxy debonding was investigated using two standard testing methods. The low shear strength of concrete near the epoxy joint was identified as the source for the weaker, stiffer and more brittle response of the mixed failure mode in the torsion tests.

1. Introduction

Concrete is one of the most widely used structural materials, and concrete structures are used in the construction of fixed onshore and offshore structures, floating offshore platforms and marine renewables structures. Due to a wide variety of applications, concrete structures are subjected to different loading conditions including torsion (e.g., in curved concrete beams). The behaviour of concrete structures under torsion has been well investigated and their failure modes have been well documented (e.g., [1–15]). Torsion causes brittle failure of concrete structures, which can be avoided by providing adequate longitudinal and transverse reinforcement.

Epoxy resins are widely used as sealing and bonding materials in various civil engineering applications including precast segmental concrete construction (e.g., [16–20]) as well as for repair and strengthening of concrete structures with externally bonded steel plates or fibre reinforced polymer wrapping (e.g., [21–29]). In the offshore renewable energy industry, post-tensioned precast segmental construction is a method promising structural and economic efficiency in the manufacturing of floating concrete structures. This construction method relies on joining concrete segments with epoxy resins. Although different jointing systems have already been developed including flat-face and shear key joints, their application in the offshore renewable energy industry has been very limited.

The behaviour of epoxy-bonded flat-face concrete joints has been investigated by several researchers e.g., [16,18], [29–35]. These studies focused on the performance of epoxy joints under tension and shear using standard and customised testing methods. The tensile behaviour of epoxy joints was also examined using the splitting test, 3-point and 4-point bending tests e.g., [30,32,34], while the shear behaviour was investigated using the slant shear test and bi-surface shear test e.g., [29,31,33,34]. The effects of different parameters on the joint bond strength were studied, which included the physical and mechanical characteristics of concrete and epoxy and the roughness of the concrete substrate. It is necessary to note that the applied testing methods had drawbacks. For example, the splitting test generated tension at the joint through the application of compression to a cylindrical specimen which introduced compressive stresses in the joint plane. The bending tests created nonuniform tensile stresses in the bottom half of the joint and nonuniform compressive stresses in the top half of the joint. The slant shear test introduced significant uniform compression stresses perpendicular to the joint plane, while the bi-surface shear test introduced nonuniform

* Corresponding author.
E-mail address: l.chernin@dundee.ac.uk (L. Chernin).

https://doi.org/10.1016/j.conbuildmat.2023.134558
Received 31 October 2022; Received in revised form 5 December 2023; Accepted 9 December 2023
Available online 16 December 2023

compression stresses normal to the joint plane over a part of its length.

To the authors' knowledge, the performance of epoxy-bonded flat-face joints under torsion has not attracted significant attention and this paper addresses this knowledge gap through a twofold experimental programme. The first part of the experimental programme investigates the static mechanical performance of a flat-face epoxy-bonded concrete jointed system subjected to torsion. Since current practice and design codes do not provide any guidelines on testing procedures for epoxy-bonded concrete joints under torsion, a custom experimental setup was developed, in which torque was applied to jointed hollow concrete prisms. The Digital Image Correlation technique was used for monitoring the development of surface strain at the joint during the tests. The torsion specimens failed in two distinct modes, one of which included partial debonding of the epoxy joint. This phenomenon was investigated further in the second part of the experimental programme using two standard testing methods. In these methods, steel and concrete were used as the substrates of the epoxy joint.

The rest of this paper is organised as follows. Section 2 describes the twofold experimental programme undertaken in this study which includes details of specimens and experimental setups used for testing the torsional capacity of concrete joints and the shear capacity of the concrete-epoxy bond. A discussion of experimental results supported by images of specimen faces and surface shear strain is presented in Section 3, where the implications of the experimental findings for the behaviour of concrete joints under torsion are also discussed. The paper ends with conclusions.

2. Experimental programme

The experimental programme consists of two types of tests examining the torsional capacity of concrete joints and the shear capacity of the concrete-epoxy bond.

2.1. Testing the torsional capacity of concrete joints

This section discusses the experimental setup of the torsion tests on flat-face epoxy-bonded concrete joints.

2.1.1. Specimens and testing rig

Due to insufficient guidelines on the subject in the practice and design codes, a custom testing method was developed for investigating the behaviour of flat-face epoxy-bonded concrete joints in torsion. The torsion test specimens consisted of two 100 mm hollow concrete cubes bonded by epoxy resin, as detailed in Fig. 1. Each specimen had a 50 mm $\times$ 50 mm square hole and 25 mm thick walls. The hole was required for the application of the torque (see the discussion of the testing rig below) and did not significantly reduce the resistance of the specimens to torsion. The concrete cubes were manufactured by cutting 200 mm long hollow prisms in half. All prisms were cured in water for 28 days after de-moulding. The surfaces of the joints were sandblasted before the application of epoxy. 9 specimens (named T1-T9) were manufactured with 3 mm thick epoxy joints. The thickness of the joints was controlled by spacers. The specimens were tested after 3 days of epoxy curing in laboratory conditions (i.e., at the temperature of 20 $\pm$ 2 °C, relative humidity of 50–60%) based on the recommendations of the epoxy manufacturer. It is necessary to emphasise that all 9 specimens were similar and had only insignificant differences unavoidable when the standard manufacturing procedures are used. It should be noted that this paper reports part of the experimental results of a larger project. The first part of the project outcomes (published by Newlands et al. [34]) investigated the shear behaviour of flat-face epoxy-bonded concrete joints, which included studying the effects of joint thickness, the epoxy material properties, surface preparation method and joint area reduction on the joint shear behaviour. The results of this parametric study and their implications for the torsional response of concrete-epoxy joints are discussed in Section 3.2.1 below.

Several types of experimental setups were developed for investigating the torsional behaviour of reinforced concrete beams. Torque was applied through lever arms to both ends of a beam using a spreader beam [3,4,9,11,12], through a lever arm to one end of the beam, while the other end was fixed [1,5–8,10,13–15] or through a lever arm to the middle of the beam, while both beam ends were fixed [2]. The torsional supports and torque application points of the beams were strengthened either by increasing the cross-section [1,2,14] or by providing additional reinforcement [3,6,7,9–11,13,15]. The beams tested in [4,5] were not strengthened, which resulted in cracking at the supports. The concrete beam ends were clamped by two parallel steel beams [4–7,9–11,13,15], fixed to a bulky concrete block [1,13,14] or encased in a steel frame [2,3]. The beam in [8] was manufactured with T-shaped ends for torque application, while the beam in [12] was manufactured with short cantilevers outstanding from the pinned supports. The loading arrangement in the beam from [12] was similar to the 4-point bending tests, which led to the development of a constant bending moment together with torsion. The loading arrangement in the beam from [2] was similar to the 3-point bending tests, which led to the development of a bending moment and shear in addition to torsion. The rotation of a loaded beam end in [3,7,10,11] required for torque application was released using a hinge provided under the support. As a result, the centre of support rotation was different in this setup from the centroid of the beam cross-section. To eliminate this drawback, the experimental setups in [5,6,9,13–15] used an arch-type support, while [1] applied torque directly to the beam using a specialised apparatus. The experimental setup in [4] did not include any rotational capabilities at the supports. The beam was simply rested on regular pinned supports, which probably caused some localised damage (not discussed by the authors).

The research studies [1–15] tested large-scale specimens. This paper

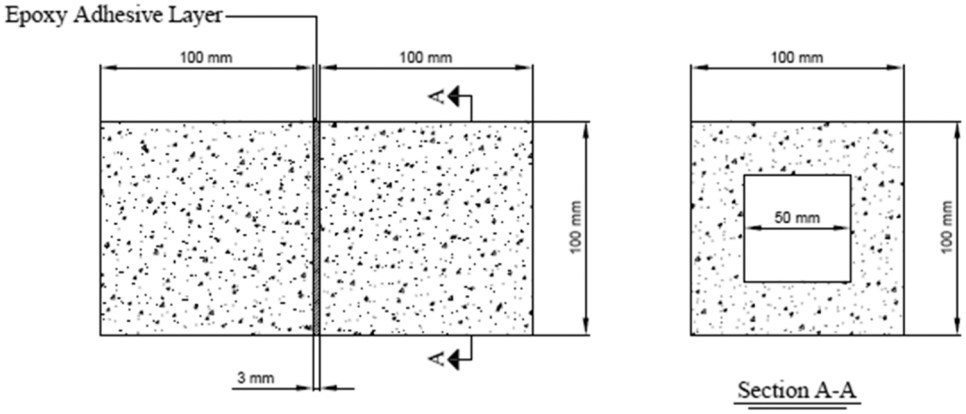

Fig. 1. Torsion test specimen.

investigated small-scale specimens, which necessitated designing and manufacturing a bespoke testing rig. The testing rig (developed for testing the specimens discussed above) consisted of two metal frames confining the cubes on both sides of the joint as shown in Fig. 2. Note that experimental setups with similar confining frames were implemented in [2,3], while similar methods of torque application through a lever arm were used in [1,5–7,10,13–15]. The frames were made of 5 steel plates covering the sides and the end faces of the cubes. Each side of the jointed concrete prism was tightened in position by 6 bolts placed in the top plate of each frame. The frames were located between two steel angled sections welded to the steel baseplate. A 224 mm long metal lever arm was welded to one of the frames holding the specimen (the left frame in Fig. 2), which could rotate around the shaft. The rotating frame additionally had a steel endplate. A central metal shaft passed through the hollow specimen, the steel endplate of the rotating frame and was supported by the angled sections. The steel end plates allowed to confine specimens against warping. The second frame was welded to the baseplate and the angled section and remained stationary (the right frame in Fig. 2). This configuration enabled the application of torque to the specimen by loading the lever arm with a standard testing machine. The force applied on the lever arm was recorded by a load cell. Two linear variable differential transformers (LVDTs) recorded the vertical and horizontal movements of one corner of the rotating frame. Additionally, a dial gauge was installed to monitor the movement of the lever arm (see

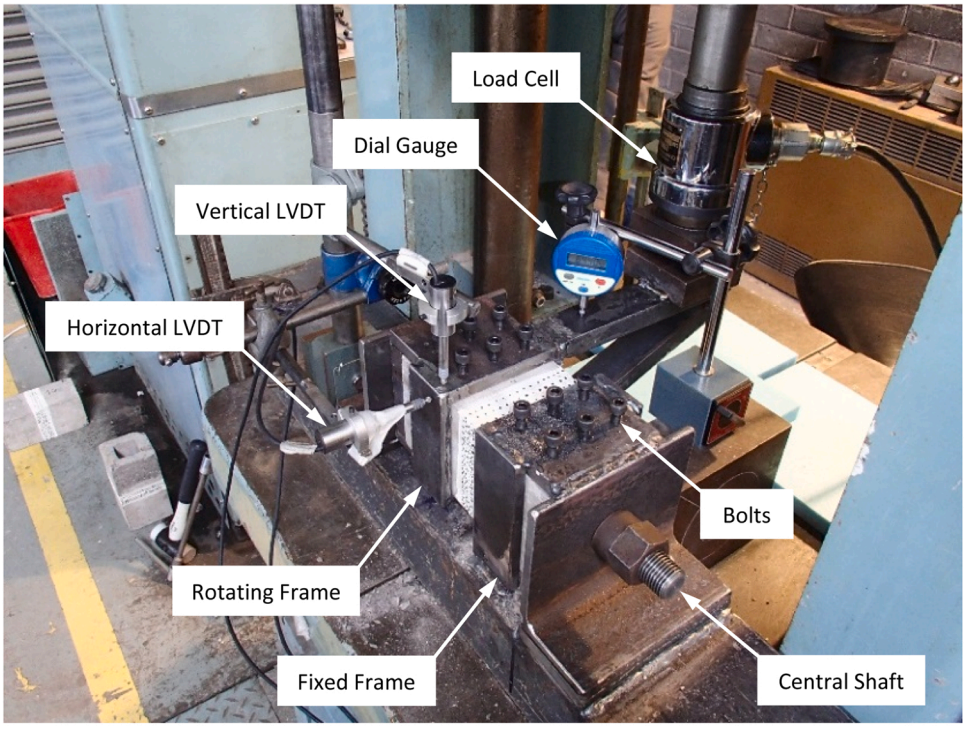

(a)

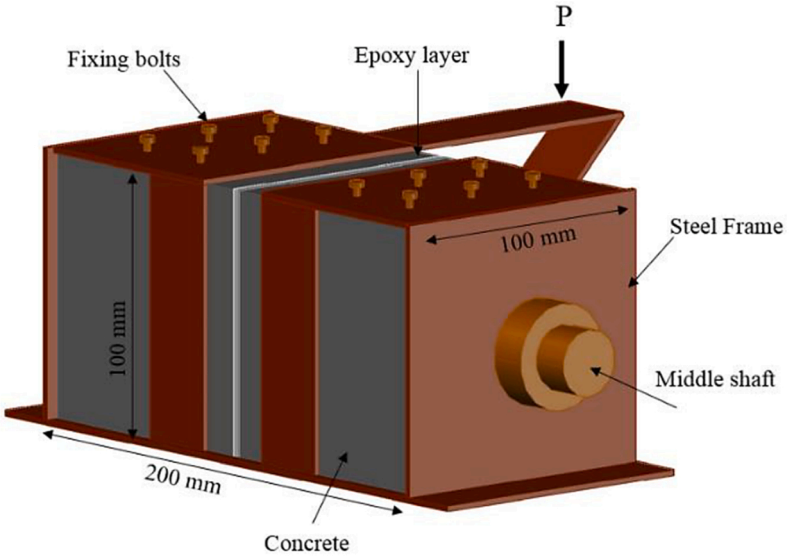

(b)

Fig. 2. Torsion test setup shown (a) during a test and as (b) a schematic model.

Fig. 2a). The data collected from the monitoring devices were used for calculating the rotation of the frame as a function of the applied torque.

It should be noted that the testing rig implemented in this study was designed with the purpose of inducing the adhesive mode of failure. This aim could have been achieved either by strengthening the concrete sections with reinforcing bars or by reducing the length of unconfined concrete. The specimen walls were too thin for any significant reinforcement, and the presence of reinforcing bars could influence the distributions of shear stresses and strains around the joint. In the second method, the confining frames applied torque nonuniformly on the specimens resulting in a nonuniform distribution of shear stresses and strains across the joint. This conclusion was supported by the development of high shear strain bands crossing the joint, which were observed with DIC (see the discussion in Section 3.1.3). Furthermore, the effect of confining frames on the experimental results could be considered relatively minor as the cracking patterns observed in the tested specimens were similar to those observed in the experimental studies [1–15]. The importance of this phenomenon for the torsional resistance of concrete joints will be further investigated in a follow-up study using numerical modelling with the finite element method. The fixing bolts (see Fig. 2) created stress concentrations, which, however, were found to be insignificant based on the indentations left on the faces of specimens tested (see Fig. 7a and supplementary materials accompanying the paper). Relatively small specimens were tested and therefore further research is required to investigate the effect of scaling on the findings of this study.

2.1.2. Strain monitoring

Digital Image Correlation (DIC) was applied during the tests for monitoring surface strains at the joint on one side of the specimen. Before testing, the surfaces of each specimen on both sides of the joint were coloured white and painted with a reference grid of black dots. Two Photron SA-1 highspeed video cameras (with a recording speed of 5400 frames per second at 1-megapixel resolution) were positioned to record the front specimen face from different angles. The captured video recordings were processed by the software VIC-3D [36], which calculated the development of surface strain fields at the joints.

2.2. Properties of materials

2.2.1. Concrete

The concrete prisms were cast using 50% GGBS concrete (C III/A) conforming to BS 8500–2 [37]. The mix design is presented in Table 1. All mixing procedures conformed to BS 1881–125 [38]. All specimens were cured for 28 days in water at the lab temperature of 20 ± 2 °C.

2.2.2. Epoxy properties

Table 2 and Table 3 present the general and mechanical characteristics of the epoxy as supplied by the manufacturers.

The energy-dispersive X-ray spectroscopy analysis of the epoxy showed that the main components of this epoxy were carbon and oxygen. Additionally, significant amounts of calcium, silicium and aluminium were present in the epoxy composition, which was attributed to the filler consisting of inorganic clay minerals. This type of filler is used to enhance the mechanical properties of epoxy and leads to roughening of its surface [39]. The scanning electron microscopy analysis conducted using Philips XL-30 microscope confirmed that the epoxy had a very rough surface texture. It should be noted that this type of filler toughened the epoxy by introducing the mechanisms of crack deflection, de-bonding of nano-clay particles and shear banding (i.e., local plastic deformation) into the fracture behaviour of the epoxy [40].

Table 2
Epoxy general characteristics (manufacturer data).

Usage Temperature (°C)	Thermal expansion, ($°C^{-1}$)	Shrinkage (%)	TG[a] (°C)	Density, (kg/l)	Mix ratio[b]
+ 8 to + 35	2.5×10^{-5}	0.04	+ 62	1.65	1:3

[a] Glass Transition Temperature
[b] Mix ratio by mass for (resin):(hardener + filler)

2.2.3. Tensile testing of bulk epoxy

The behaviour of the epoxy in tension was assessed using a dogbone specimen manufactured from bulk epoxy. The testing methodology conformed to ASTM D638 [41] test method for tensile properties of plastics. Type I specimen suitable for rigid and semi-rigid plastics was selected. The specimen is shown in Fig. 3 and its dimensions are given in Table 4.

The dogbone specimen was cast in a prefabricated aluminium mould. A release agent for cold mounting materials like epoxies was used to avoid sticking the specimen to the mould. The specimen was cured at the lab temperature of 20 ± 2 °C for three days, after which it was demoulded and tested using INSTRON 5985 with a mounted 50 kg load cell and LVDTs. As per ASTM D638 [41] recommendations, the distance between the INSTRON grips was 115 mm (see Fig. 3b). The specimen ends were wrapped with sandpaper to avoid stress concentrations in the grips. The test was conducted at the loading rate of 2 mm/min. The extension was measured over the 50 mm gauge length in the specimen's narrow part using an extensometer (see Fig. 3b). Fig. 4 shows the stress-strain curve obtained based on the tensile test data.

As can be seen, the stress-strain curve in Fig. 4 is close to linear, which is characteristic of brittle behaviour exhibited by rigid plastics. The tensile strength of the tested specimen was 28.8 MPa. The analysis of the initial part of the curve yielded Young's modulus of 14.5 GPa. As a result, the tested specimen showed higher values of tensile strength and stiffness (i.e., Young's modulus) than those supplied by the manufacturer, see Table 3. It should be noted that because only one epoxy specimen was tested, the obtained data can only be considered as an indication that the mechanical properties provided by the manufacturer are correct.

2.3. Testing the shear capacity of concrete-epoxy bond

The test of the shear capacity of the concrete-epoxy bond was implemented to understand the effect of local debonding of the epoxy layer that occurred due to shear on the torsional capacity of the entire flat-face epoxy-bonded concrete joint. The investigation of the shear strength of the concrete-epoxy bond was carried out using the assumption that the bonding strength of the epoxy to steel is about 5 times higher than that of concrete. This assumption was based on the manufacturer data in Table 3 for the bonding strength of the epoxy to concrete and steel in the direction normal to the joint plane (see footnote 1 of

Table 1
Test concrete mix proportions and selected properties.

Constituent Proportions (kg/m^3)					SP[b] (%)	Selected Properties			
CEM I 52.5 N	GGBS	Water	Aggregates[a] Fine (0/5)	Coarse (5/20)		w/c ratio	Plastic Density (kg/m^3)	Slump (mm)	$f_{c,cube}$[c] (MPa)
225	225	170	680	1090	0.4%	0.38	2390	100	60

[a] Coarse aggregate and granite fine aggregate glacial sand (1% water absorption)
[b] Superplasticizer, % of total cementitious material by weight
[c] Cube compressive strength at 28 days after casting

Table 3
Epoxy mechanical characteristics (manufacturer data).

Strength characteristics (MPa)				Moduli characteristics, GPa			Fracture thoughness[b] (N/m)
Compressive	Shear	Tensile	Bond[a]	E_{compr}	$E_{tensile}$	G_{shear}	
65-75	13-16	21-24	> 4	9.6	11.2	1.5	6368

[a] On concrete, based on substrate failure (bond strength on steel > 21 MPa)
[b] For Mode I (opening)

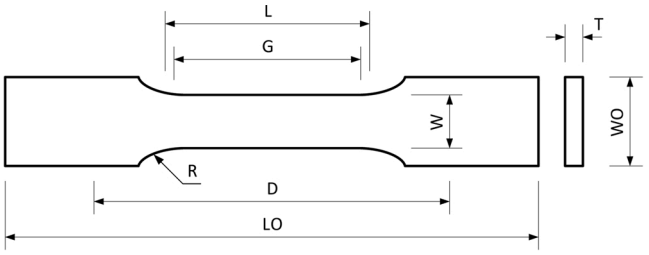

(a)

(b)

Fig. 3. (a) Type I specimen, as per ASTM D638 [41]. The dimensions are given in Table 4. (b) The testing setup of the dogbone specimen.

Table 4
Dogbone bulk epoxy specimen dimensions, as per Type I specimen in ASTM D638 [41].

Designation	Parameter	Dimension (mm)
T	Thickness	3.2 ± 0.4
W	Width of narrow section	13
L	Length of narrow section	57
WO	Width over all	19
LO	Length over all	165
G	Gauge length	50
D	Distance between grips	115
R	Radius of fillet	76

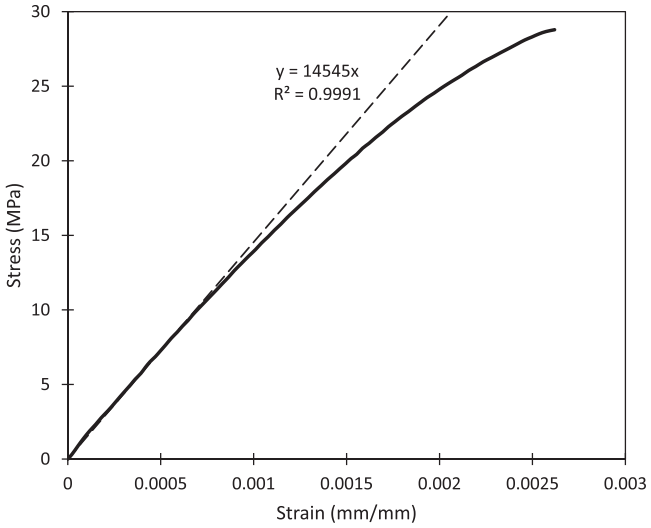

Fig. 4. Results of tensile test on a dog-bone epoxy specimen.

Table 3).

2.3.1. Push and pull testing methods

The flat-face epoxy-bonded concrete joint can fail either in concrete, joint epoxy layer or at the concrete-epoxy interface. The non-uniform, composite nature of concrete resulted in stiffness variations at the joint surface leading to stress concentrations. The shear behaviour of the concrete-epoxy bond was investigated in this study using the Push and Pull testing methods, where concrete was bonded by epoxy to steel. This reduced the effect of stress concentrations and allowed to achieve a more uniform distribution of shear stresses over the joint length. The Push and Pull tests provided new insights into the shear response of the concrete-epoxy joint as they eliminated the disadvantages of the slant and bi-surface shear test setups implemented by Newlands et al. [34] that laid in the presence of compression force at the joint and the nonuniform distribution of shear stresses at the joint.

In the Push test method, a steel I-beam was sandwiched between 2 concrete slabs. The beam had a depth of 100 mm and a flange width of 80 mm. The concrete slabs were 300 mm long, 300 mm wide and 100 mm deep. The slabs were cured in water for 28 days after de-moulding. The beam was bonded to the concrete slabs with the epoxy over 100 mm length and the entire width of the flanges as shown in Fig. 5. The surfaces of concrete slabs and steel beams were sandblasted before bonding. Spacers were used to control the thickness of the joints. Based on the recommendations of the epoxy manufacturer, the specimens were cured for 3 days after bonding at the lab temperature of 20 ± 2 °C and relative humidity of 50–60%s. The top of the beam was pushed by a standard testing apparatus between the concrete slabs creating shear stresses at the steel-concrete joints. The beam and slabs were well aligned during manufacturing to avoid the eccentricity of the applied load. The symmetry of the Push test specimen allowed to generate a pure shear stress state. Four LVDTs were installed on each side of the joints to record the slip of the beam relative to the concrete slabs. A load cell was located on top of the beam for monitoring the

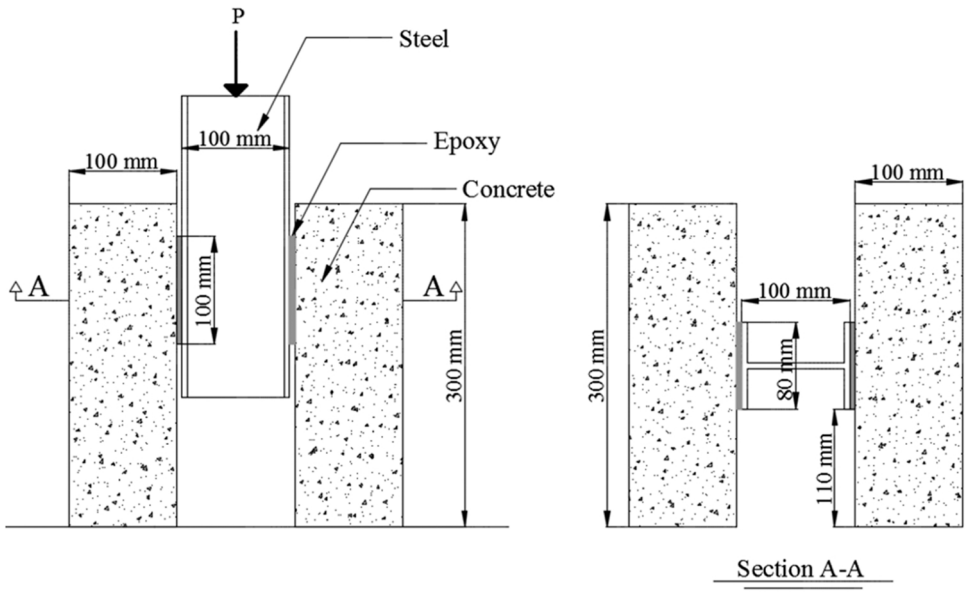

Fig. 5. Push test specimen.

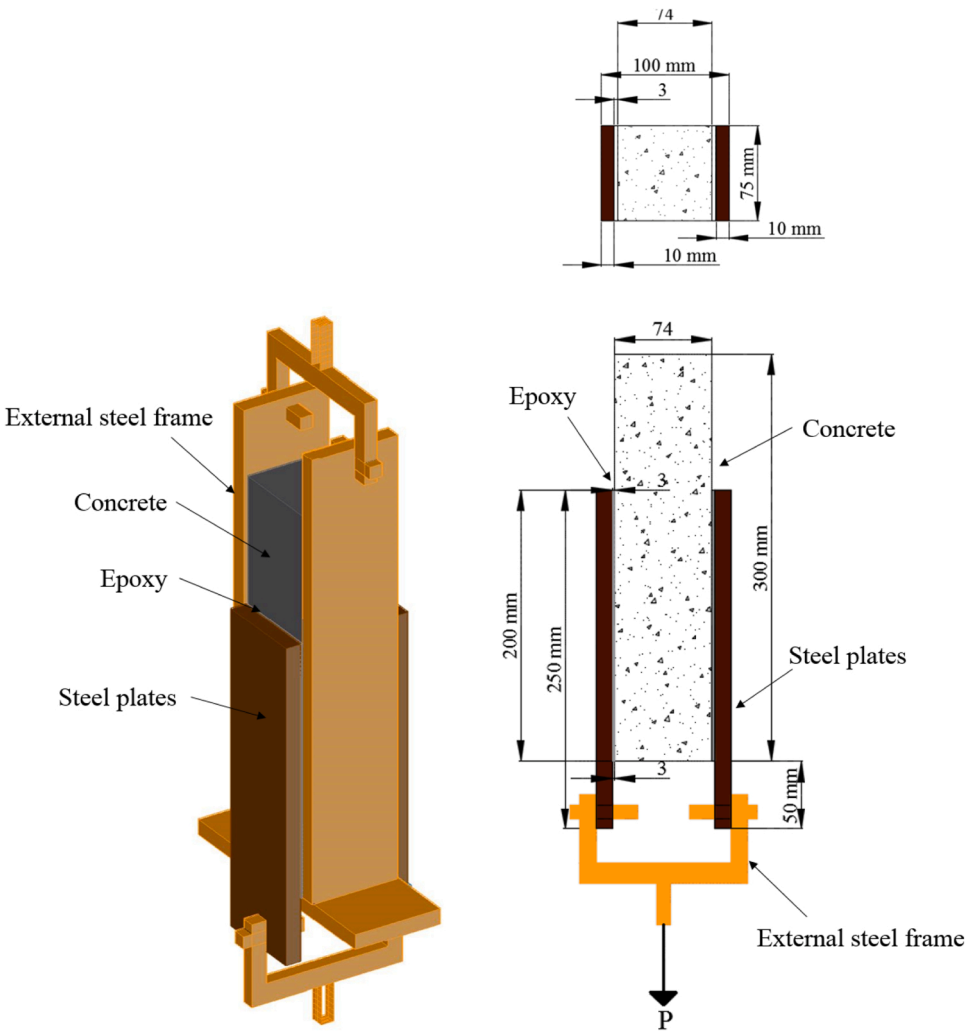

Fig. 6. Pull test specimen and confining steel frame.

applied load. The Push test was carried out on 3 specimens. It should be noted that a similar method was used by Eurocode 4 [42] for testing the strength of shear connectors and by Si Larbi et al. [43] for testing the effect of paint on the failure mode and strength of the steel-concrete joint.

Since the Push test could be affected by the compression stresses in the beam and the wedging action, an alternative Pull test method was additionally used for validating the shear strength of the concrete-epoxy bond. In the Pull test method, a concrete prism was clamped in a steel frame, as shown in Fig. 5. A pair of steel plates were bonded to the opposite sides of the prism. These plates were pulled using an additional steel frame creating a state of pure shear stresses in the steel-concrete joints. In the Pull test specimen, the prisms were 300 mm long and had a 75 mm × 75 mm cross-section. The steel plates were 250 mm long, 75 mm wide and 10 mm deep. The prisms were cured in water for 28 days after de-moulding. The surfaces of concrete prisms ans steel plates were sandblasted. After epoxy application and bonding of prisms with plates, the specimens were cured for a further 3 days in laboratory conditions. It should be noted that a similar method was applied by Barnes and Mays [21] in investigating the potential for strengthening reinforced concrete beams with externally bonded steel plates. The authors reported that the efficient bonding length is between 100 mm and 200 mm. Therefore, the plates were bonded to the prism over the length of 200 mm and the entire prism breadth. The bonded plates were aligned with the prisms to avoid the eccentricity of the applied load. Two LDVTs were applied to monitor the slip of the plates relative to the prism. The applied load was recorded using a load cell. The Pull test was carried out on 3 specimens.

It is necessary to mention that all specimens in both types of tests were manufactured using the concrete and the epoxy described in Section 2.2. The epoxy layers in all steel-concrete joints were 3 mm thick..

3. Experimental results and discussion

3.1. Torsional capacity of concrete joints

This section presents the results of torsion tests on 9 similar specimens discussed in Section 2.1.

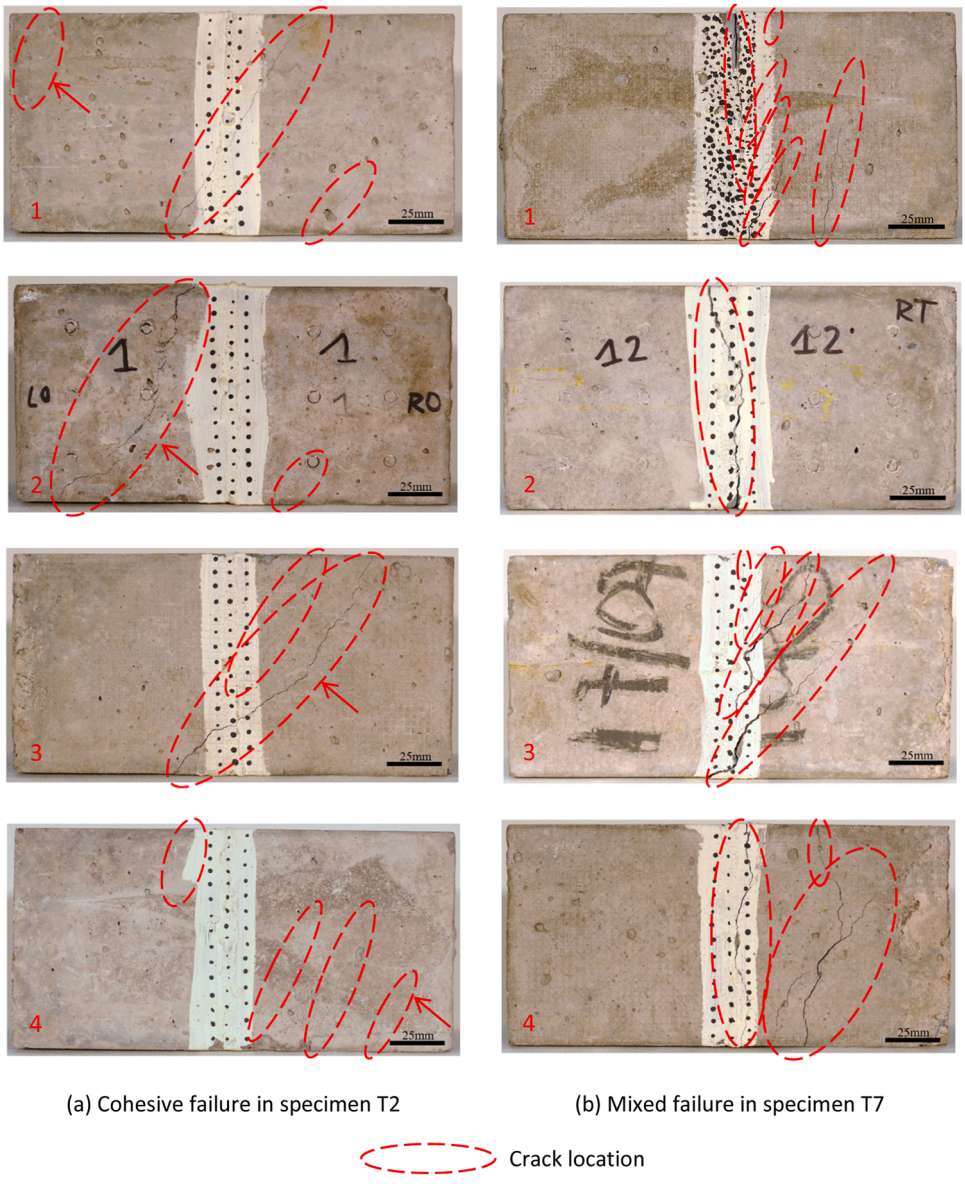

Fig. 7. Failure modes observed in torsion tests. From top to bottom, images are given for the (1) front, (2) top, (3) back and (4) bottom faces of specimens. The scale bar in the right bottom corner of each image represents 25 mm in length.

3.1.1. Failure modes observed in torsion tests

Despite being similar, the torsion test specimens exhibited two different modes of failure: cohesive and mixed. The cohesive mode was characterised by the failure in the body of concrete on one side or both sides of the joint. The mixed mode was characterised by the failure in the body of concrete on one side of the epoxy joint and partial debonding of the joint. The adhesive failure mode (i.e., the failure of the epoxy layer) was not observed in the tests. It should be noted that the differences in the failure modes observed in the torsion tests stem from the variations in the distributions of mechanical properties within the specimens. These include the variations in the strength and stiffness of the concrete at the joint surface and in the bond strength of the concrete-epoxy interface. Typical examples of the cohesive and mixed failure modes are shown in Fig. 7, where dashed ovals indicate the locations of cracks. Since the adhesive mode of failure (i.e., failure purely occurring in the epoxy joint) was not observed it could be concluded that the torsional shear strength of the epoxy was higher than that of the hollow concrete cubes. The cohesive failure mode was dominant, occurring in 6 out of 9 specimens (see Table 5). In this mode, several cracks developed in the specimen with most of them inclined to the axis of rotation at inclination angles ranging between 30° to 60° (see Fig. 7a and supplementary materials accompanying the paper). Many cracks continued over several specimen faces in a spiral pattern, where the change of specimen face was often accompanied by a change in the crack inclination angle. An example of a spiral crack extending over all 4 faces of specimen T2 is indicated by arrows in images 1–4 of Fig. 7a. It should be noted that similar crack patterns were observed in torsion tests on solid and hollow reinforced concrete beams (e.g., [1–15]). At least one inclined crack crossed the joint in each specimen, while some inclined cracks stopped at the joint (see images 1 and 3 of Fig. 7a). In most cases, the crack crossed the joint perpendicularly after a short propagation along the concrete-epoxy interface. The direction of the joint-crossing crack within the concrete cubes was similar on both sides of the joint.

The mixed mode failure occurred in 3 out of 9 specimens (i.e., in specimens T3, T5 and T7, see Table 5). In specimens T3 and T5, cracks developed in one of the jointed cubes and in the concrete near the joint without crossing the latter (see Fig. 7b and supplementary materials accompanying the paper). In specimen T7, one crack crossed the joint twice on two adjacent faces (see images 2 and 3 of Fig. 7b). Out of 3 specimens, specimen T7 was the most severely damaged. In the concrete near the joint, cracks developed in parallel to the joint plane and became inclined away from the joint (see images 1 and 3 of Fig. 7b). The inclination angles of the cracks to the axis of rotation ranged between 45° to 70°. In the bulk concrete, the inclined cracks continued to adjacent faces, with some inclined cracks becoming perpendicular to the axis of rotation (see images 1 and 4 of Fig. 7b). Most inclined cracks connected with joint cracks that continued over two or three specimen faces with local debonding at the concrete-epoxy interface. Note that the debonding occurred by the failure of the concrete surface layer rather than the epoxy and a thin layer of concrete remained attached to the epoxy after the test.

The images of specimens T1, T3-T6 and T7 are given in the supplementary materials accompanying the paper.

3.1.2. Torsional strength

The torsion test specimens were hollow prisms with a 100 mm × 100 mm cross-section and 25 mm thick walls. Assuming a linear distribution of shear stress within the cross-section, the contribution of the 50 mm × 50 mm core to the torsional resistance of a torsion test specimen can be considered as relatively small and can be ignored. Therefore, ACI-ASCE Committee 445 [44] allows considering such prisms as solid, where the torsional stresses, τ, is continuous in the cross-section and can be calculated using the following expression

$$\tau = \frac{T}{\alpha \sum x^2 y} \tag{1}$$

$$\alpha = [3 + 1.8x/y]^{-1} \tag{2}$$

where T is the applied torque, x and y are specimen cross-section dimensions, and α is a coefficient dependent on these dimensions. In the considered case, $x = y = 100$ mm and so Eq. (2) results in $\alpha = 0.208$ and Eq. (1) leads to

$$\tau = 4.8 \times 10^{-6} \times T \tag{3}$$

where τ is in MPa and T is in N•mm.

Fig. 8 presents the development of τ with the rotation of the section in the specimens tested, while Table 5 gives the values of τ, cross-sectional rotation and rotational deflection at specimen failure. The torsional stress was calculated using Eq. (3), where T was obtained using the load cell readings as the load applied by the testing machine times the distance (i.e., lever arm) between the point of load application and the axis of the steel shaft (see Fig. 2). The rotation of the cross-section was evaluated as the rotational deflection divided by the lever arm of the applied load, where the rotational deflection was calculated as the square root of the sum of squares of the readings made by the two LVDTs installed in the vertical and horizontal directions (see Fig. 2a). It is necessary to note that rectangular cross-sections under torsion are affected by warping, however, the restrains at the ends of the specimen in the frame meant that this effect was insignificant. As can be seen in Fig. 8, specimens T2, T3, T4, T7, T8 and T9 exhibited slip in the confining frame at the beginning of the tests, which lead to low inclinations in the initial parts of their curves. Since all specimens failed in a brittle manner, the distribution of shear stress in the section remained close to linear at failure and Eq. (3) can be used to evaluate the specimen tortional strength. The average torsional strength of the specimens with the mixed failure was 4.1 MPa and the corresponding average sectional rotation at failure was 0.22° (see Table 5). The specimens with the cohesive mode failure showed a slightly higher average torsional strength of 4.4 MPa and a higher sectional rotation of 0.34°. As a result, the mixed mode failure was on average weaker and less ductile than the cohesive failure. The inclination angles of the mixed failure curves were higher on average, which indicated that the mixed failure mode was stiffer than the cohesive failure mode.

Table 5
Torsion test results.

Specimen	Failure mode	Failure stress (MPa)	Average failure stress (MPa)	Rotational deflection at failure (mm)	Rotation at failure (degrees)	Average rotational (degrees)
T1	Cohesive	5.28	4.4	0.57	0.46	0.34
T2	Cohesive	3.78		0.33	0.27	
T4	Cohesive	4.92		0.54	0.44	
T6	Cohesive	3.96		0.50	0.41	
T8	Cohesive	4.74		0.30	0.25	
T9	Cohesive	3.58		0.23	0.19	
T3	Mixed	4.42	4.1	0.34	0.27	0.22
T5	Mixed	3.97		0.25	0.21	
T7	Mixed	3.89		0.24	0.19	

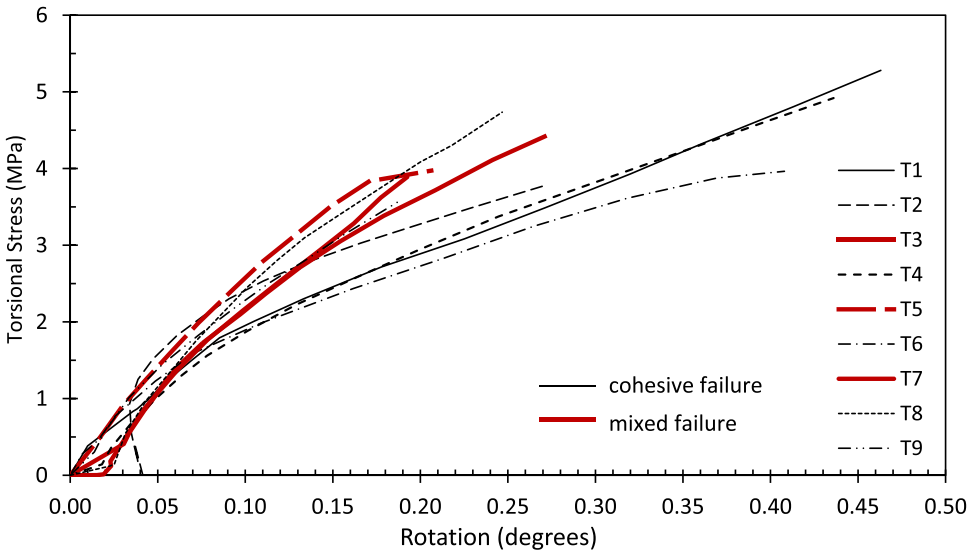

Fig. 8. Torsional stress vs. rotation.

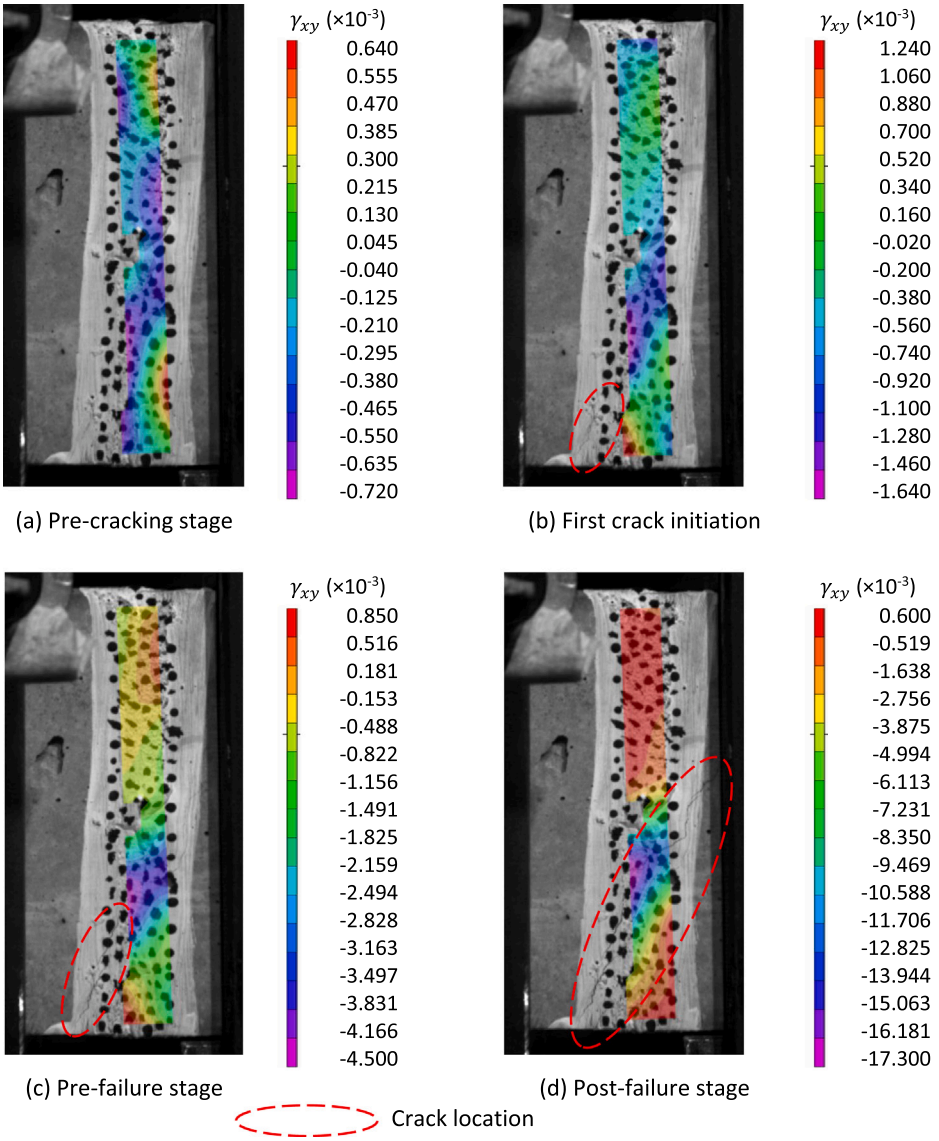

Fig. 9. Surface shear strain γ_{xy} distribution on front face of specimen T6 during cohesive failure.

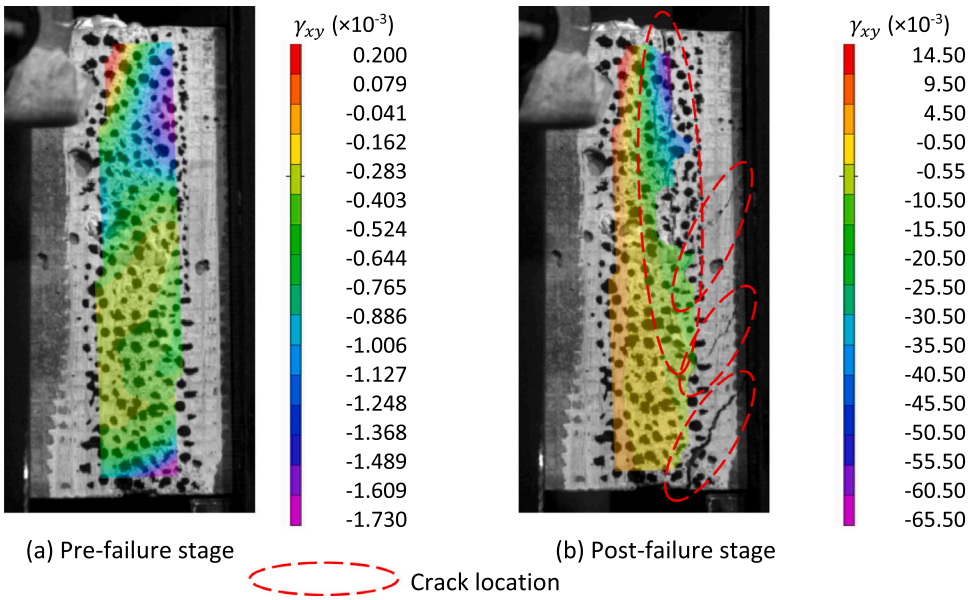

Fig. 10. Surface shear strain γ_{xy} distribution on front face of specimen T7 during mixed failure.

3.1.3. Surface shear strain

Fig. 9 and Fig. 10 present the distributions of the surface shear strain, γ_{xy}, across the joint obtained using the DIC method for different stages of testing the specimens T6 and T7. Dashed ovals indicate the locations of cracks in both figures. Note that specimen T6 failed with the cohesive mode, while specimen T7 failed with the mixed mode.

Fig. 9 depicts four stages of specimen T6 response to torsion including the pre-cracking strain stage, the stage at the initiation of the first inclined crack as well as the pre- and post-failure stages. As can be seen in Fig. 9a, a zone of high shear strain (reaching $\gamma_{xy} = -0.00072$) developed in the lower half of the joint. This zone was part of a high shear strain band passing through the joint and inclined at about 60° to the axis of rotation. The development of this band led to the initiation of the first inclined crack at the bottom side of the specimen as shown in Fig. 9b when the maximum strain at the joint reached $\gamma_{xy} = -0.00164$. The cracking process was gradual and continued with growing and branching of the first crack along the high shear strain band towards the joint. Fig. 9c depicts the pre-failure stage (with $\gamma_{xy} = -0.00450$ in the joint) just before the growing crack reached the joint. Failure of the specimen corresponded with the crack passing through the joint. Fig. 9d shows the shear strain distribution after specimen failure when the maximum strain at the joint reached $\gamma_{xy} = -0.01730$. The presence of the joint did not compromise the monolithic behaviour of the specimen under torsion. However, the joint introduced a local change in the direction of the crack, which crossed the joint perpendicularly to its plane. Although the inclined cracks were typical for the considered loading conditions, the development of non-uniform shear strain distribution with inclined high shear strain bands could be caused in the joint by the proximity of the confining steel frames applying torque nonuniformly on the specimen.

Fig. 10 depicts the shear strain distribution along the joint in the pre- and post-failure stages of specimen T7. Two zones of high shear strain (reaching $\gamma_{xy} = -0.00173$) at the top and bottom of the joint developed at the pre-failure stage (see Fig. 10a). These zones were parts of inclined high shear strain bands. The presence of the joint did not introduce any localised concentrations in the surface shear strain distribution and the specimen behaved monolithically until failure. The failure of specimen T7 was immediate with the main crack developing in the concrete along the joint from the top zone of high shear strain and three inclined cracks developing along the joint from its bottom right (see Fig. 10b and image 1 in Fig. 7b). Partial debonding at the epoxy joint occurred (see images 1 and 2 of Fig. 7b). The cracks in the right concrete cube were inclined at about 45° to the axis of rotation. The shear strain reached $\gamma_{xy} = -0.0655$ at the top of the joint.

It is important to note that the gradual nature of the cohesive failure mode and the immediate nature of the mixed failure mode indicate the development of different failure mechanisms. This is supported by the conclusion made based on the analysis of Fig. 8 that the mixed failure mode is stiffer and less ductile than the cohesive failure mode.

3.2. Shear capacity of concrete-epoxy bond

As discussed in Section 3.1.1, the mixed failure mode of the joint in torsion was accompanied by local debonding of the epoxy and concrete which occurred due to shear (see Fig. 7b and Fig. 10b). The effect of local debonding of the epoxy layer on the concrete-epoxy bond strength was examined using the existing experimental data reported by Newlands et al. [34] and new experimental data from the Push and Pull tests discussed in Section 2.3.1.

3.2.1. Concrete bonded to concrete

Table 3 contains information from the manufacturer on the strength of the bond between the epoxy and concrete in the direction normal to the joint plane. The shear strength of the flat-face concrete joints bonded by epoxy was investigated by Newlands et al. [34] using the slant and bi-surface shear tests. Several slant and bi-surface shear specimens tested in Newlands et al. [34] were made of the same concrete as the torsion test specimens in this study and their joint surfaces were sand-blasted and bonded with the same epoxy (i.e., epoxy B in [34]). The specimens with 3 mm thick joints exhibited either the adhesive failure mode (i.e., failure in the epoxy layer) or the cohesive failure mode (i.e., failure in the concrete on one or both sides of the joint), where the cohesive failure mode was more dominant. The slant shear test specimens showed a shear strength of 10.9 MPa at the adhesive failure and a shear strength of 10.1 MPa at the cohesive failure. The bi-surface shear test specimens showed a shear strength of 7.48 MPa at the adhesive failure and a shear strength of 5.43 MPa at the cohesive failure. As a result, the shear strength of the concrete-epoxy bond depends on the experimental setup and failure mode. As discussed in Newlands et al. [34], both types of shear tests generated non-uniform distributions of shear stresses along the joint, although the distribution of shear stresses in the bi-surface shear test was more even. Compression stresses normal

to the epoxy joint developed in the slant shear test specimens due to the experimental setup arrangement. A low span-depth ratio (close to 1) of the bi-surface shear test specimen introduced the arching effect which led to the development of compression stresses over a part of the joint. Since the shear strength in the slant shear tests was higher than in the bi-surface shear test, it can be concluded that the compression stresses were higher in the former test and distributed over a relatively larger part of the joint. Therefore, the results of the slant shear test are not directly applicable to the analysis of the torsion strength of the concrete-epoxy joint. The average shear strength of 5.43 MPa obtained in the cohesive failure mode in the bi-surface shear test is relatively close to the average torsional strength of 4.4 MPa obtained in the same failure mode (see Section 3.1.2 and Table 5). Since the torsion test specimens did not fail with the adhesive mode, the results of the torsion tests cannot be compared with the higher shear strength of the epoxy-bonded concrete joint in the adhesive failure mode obtained in the bi-surface shear test.

Newlands et al. [34] also reported that the increase of joint thickness increased the occurrence of adhesive shear failure with a rate of over 10% per 1 mm thickness increase. It can therefore be assumed that the increase in joint thickness would result in the mixed failure mode becoming dominant and the occurrence of the adhesive failure mode becoming probable. This assumption, however, is questionable as it is based on the conclusion obtained disregarding the method of joint surface preparation and the epoxy mechanical properties. It was also suggested above that the results of the slant shear test could not be directly applicable to the analysis of the torsion strength of the concrete-epoxy joint due to the presence of compression stresses at the joint. Furthermore, the bi-surface shear test data did not demonstrate a similar relationship between joint thickness and failure mode.

The data describing the effect of the epoxy material properties (i.e., epoxy shear and bond strength) and the method of joint surface preparation (i.e., no preparation, sandblasting and wire brushing) on the joint shear strength was inconsistent, which prevented Newlands et al. [34] from establishing any clear relationships.

Newlands et al. [34] also investigated the effect of the joint area reduction (including 10% and 50% debonding) on the joint shear behaviour using the bi-surface shear test. It was reported that the area reduction weakened the joint. The loss of shear strength of a 2 mm thick joint was comparable to the debonded area, i.e., a 10% debonding resulted in a 15.3% strength loss, while a 50% debonding resulted in a 53.5% strength loss. For the joint with a 10% debonded area, the 1 mm increase in thickness increased its strength by about 7% leading to a nearly complete strength recovery in the 4 mm thick joint. The 1 mm increase in the thickness of the joint with 50% area debonding resulted in an about 16% strength increase leading to the recovery of more than half of the lost strength in the 4 mm thick joint. Therefore, it can be assumed that the increase in joint thickness can compensate the loss of torsional strength due to partial joint debonding.

A parametric study investigating the effects of aforementioned parameters on joint torsional response is necessary to establish accurately the governing parameters and most sensitive ranges of values. Numerical modelling using the finite element method is most suitable for this purpose as it will allow to explicitly control parametric values.

3.2.2. *Concrete bonded to steel*

All specimens in the Push and Pull tests failed with the cohesive mode by the cracking of concrete along the joint. After the failure, a thin layer of concrete was still attached to the epoxy joint. This concrete layer contained only cement paste and fine aggregate, while coarse aggregate remained attached to bulk concrete. Typical states of specimens after the Push and Pull tests are shown in Fig. 11, where the concrete layers attached to the epoxy joints are visible in both types of tests. In Fig. 11a, one slab was removed after specimen failure to show the joint. It is important to note that the occurrence of the cohesive failure mode of the steel-concrete joint in all specimens tested justified the assumption that the bonding strength of the epoxy to steel is much higher than to concrete. In both types of tests, the slip displacement of the steel-concrete joint at specimen failure was smaller than 0.25 mm (in most cases significantly smaller than this value). This indicated that the response of the steel-concrete joint was very stiff. The average shear strength of the steel-concrete joint was 1.73 MPa in the Push tests and 1.75 MPa in the Pull tests. The consistency in the shear strength values suggests that both types of tests generated a similar shear stress state at the steel-concrete joint.

As can be observed, the shear strength of the concrete-epoxy bond obtained in the Push and Pull tests is much lower than that obtained in the slant and bi-surface shear tests reported in Newlands et al. [34] and discussed in Section 3.2.1. Possible reasons for the divergence of shear strength include fundamental differences in the experimental setups.

Fig. 11. Typical cohesive failure modes of (a) Push and (b) Pull tests.

The slant and bi-surface shear tests created non-uniform distributions of shear stresses along the joints as well as applied compression stresses at the joints perpendicularly to the joint plane. In contrast, the steel side of the joint in the Push and Pull tests (i.e., steel beam flange or steel plate, respectively) was very stiff relative to the concrete side (i.e., concrete slab or concrete prism) leading to a more uniform distribution of shear stresses along the joint. The Push and Pull tests did not introduce compression stresses normal to the joint plane and the shear strength of the concrete-epoxy bond was not enhanced. Consequently, the actual shear strength of the concrete-epoxy bond could be lower than the previously reported values, e.g., in Newlands et al. [34]. This conclusion is supported by the results of the torsion tests, in which the specimens had a lower average torsional strength of 4.1 MPa in the mixed failure mode (compared to 4.4 MPa in the cohesive failure mode) due to partial debonding of the joint by cracking of adjacent concrete (see Sections 3.1.1 and 3.1.2). In addition, this also explains the stiffer and more brittle response of the mixed failure mode as the concrete-epoxy debonding is a stiffer and more brittle action than torsional shear cracking of concrete. During the mixed mode failure of torsion test specimens, cracks developed along the joint from the high shear zones because the shear strength of the joint was low. The partial nature of joint debonding is the result of the nonuniform application of torque by the torsion rig, which led to the development of bands of high shear stresses in the specimens. These conclusions are supported by the DIC observations discussed in Section 3.1.3. It should also be noted that the debonding of steel-concrete and concrete-concrete joints were accompanied by a layer of concrete left on the joint after specimen failure. This suggests that the failure mechanisms governing the Push and Pull tests were also present in some torsion tests.

4. Conclusions

This paper investigated the torsional capacity of flat-face concrete joints bonded by epoxy using a custom experimental setup. The analysis of the experimental results yielded the following conclusions:

- The specimens failed either in the cohesive or mixed mode, where the former mode was dominant. The cohesive failure mode was characterised by the development of cracks in the concrete on one or both sides of the joint, while the mixed failure mode was characterised by partial debonding of the joint and by the development of cracks in the concrete on one side of the joint.
- In both failure modes, the cracks developed either perpendicularly or at an angle to the axis of rotation. Most of the crack inclination angles were in the range between 30° to 60° in the cohesive failure mode and between 45° to 70° in the mixed failure mode. The cracks usually extended over 2 or 3 sides of the specimen in a spiral style, often with changing the inclination angle. At least one inclined crack always passed through the joint in the cohesive failure mode. The epoxy joint affected locally the direction of the crack. In the mixed failure, the inclined cracks were usually connected to the main crack passing along the joint.
- The mixed failure mode specimens were weaker in torsion and exhibited a stiffer and more brittle response than the cohesive failure mode specimens. Bands of high shear strain crossing the joint at angles between 45° to 60° were detected using the DIC method. The partial debonding of the joint in the mixed failure mode originated at one of the high shear strain bands.

The bonding strength of the epoxy to concrete was investigated using the Push and Pull tests. The results of these tests led to the following findings:

- All specimens in both types of tests failed by debonding in the concrete near one of the two joints. The shear strength of the concrete-epoxy bond was similar in both types of tests but weaker than the values reported earlier in scientific literature.
- The inherent weakness of the concrete-epoxy bond caused partial debonding of the joint in the zones of high shear strain observed in the torsion test specimens that failed with the mixed mode. The stiff and brittle nature of the concrete-epoxy bond failure explained the stiffer and more brittle behaviour of specimens that failed with the mixed mode.

CRediT authorship contribution statement

Newlands Moray: Supervision, Methodology, Conceptualization. **Khosravi Noushin:** Visualization, Validation, Investigation. **Chernin Leon:** Writing – review & editing, Writing – original draft, Formal analysis.

Declaration of Competing Interest

All authors of a manuscript titled "Flat-Face Epoxy-Bonded Concrete Joints Loaded in Torsion: Physical modelling" declare that they have no known competing financial interests or personal relationships that could have appeared to influence the work reported in this paper. Also, the authors declare that there are no financial interests/personal relationships which may be considered as potential competing interests.

Data availability

Data will be made available on request.

Acknowledgements

The authors would like to express their gratitude to Mr Jon Benzie senior engineer at Quoceant Ltd. for his valuable input to this project, also acknowledge the hard work and help of all the students at the University of Dundee who conducted sample preparation and testing. Special thanks to the epoxy manufacturer who supplied materials samples and the EPSRC Engineering Instrument Pool which supplied the DIC cameras and software.

References

[1] S.M.R. Lopes, L.F.A. Bernardo, Twist behavior of high-strength hollow beams – formation of plastic hinges along the length, Eng. Struct. 31 (1) (2009) 138–149.
[2] S.B. Talaeitaba, D. Mostofinejad, Fixed supports in assessment of RC beams' behavior under combined shear and torsion, Int. J. Appl. Sci. Technol. 1 (5) (2011) 119–126.
[3] C.E. Chalioris, C.G. Karayannis, Experimental investigation of RC beams with rectangular spiral reinforcement in torsion, Eng. Struct. 56 (2013) 286–297.
[4] J. Al-Khafaji, I. Al-Shaarbaf, R.F. Abbas, Torsional behavior of steel fibers reinforced self-compacting concrete beams, J. Eng. Dev. 19 (3) (2015) 62–80.
[5] J. Kim, M. Kwon, H. Seo, J. Lim, Experimental study of torsional strength of RC beams constructed with HPFRC composite mortar, Constr. Build. Mater. 91 (2015) 9–16.
[6] M.Y. Alabdulhady, L.H. Sneed, C. Carloni, Torsional behavior of RC beams strengthened with PBO-FRCM composite- an experimental study, Eng. Struct. 136 (2017), 393e405.
[7] K. Shen, S. Wan, Y.L. Mo, A. Song, X. Li, Behavior of single-box multi-cell box-girders with corrugated steel webs under pure torsion. Part I: experimental and numerical studies, Thin-Walled Struct. 129 (2018), 542e57.
[8] C.-H. Jeng, M. Chao, H.-C. Chuang, Torsion experiment and cracking-torque formulae of hollow prestressed concrete beams, Eng. Struct. 196 (2019), 109325.
[9] C. Joh, I. Kwahk, J. Lee, I.-H. Yang, B.-S. Kim, Torsional behavior of high-strength concrete beams with minimum reinforcement ratio, Adv. Civ. Eng. (2019), 1432697.
[10] Ibrahim, A., Askar, H.S. and El-Zoughiby, M.E. Torsional behavior of solid and hollow concrete beams reinforced with inclined spirals. Journal of King Saud University – Engineering Sciences, 2020.
[11] R.F. Hassan, N.H. Al-Salim, N.S. Mohammed, H.H. Hussein, Experimental study and theoretical prediction on torsional strength with different steel fiber reinforced concretes and Cross-Section areas, Eng. Struct. 251 (2022), 113559.
[12] A. Karimipour, J. De Brito, M. Ghalehnovi, O. Gencel, Torsional behaviour of rectangular high-performance fibre-reinforced concrete beams, Structures 35 (2022) 511–519.

[13] J. Zhou, C. Li, Z. Feng, D.-Y. Yoo, Experimental investigation on torsional behaviors of ultra-high-performance fiber reinforced concrete hollow beams, Cem. Concr. Compos. 129 (2022), 104504.
[14] C. Zhou, J. Wang, W. Jia, Z. Fang, Torsional behavior of ultra-high performance concrete (UHPC) rectangular beams without steel reinforcement: experimental investigation and theoretical analysis, Compos. Struct. 299 (2022), 116022.
[15] C. Zhou, J. Wang, X. Shao, L. Li, J. Sun, X. Wang, The feasibility of using ultra-high performance concrete (UHPC) to strengthen RC beams in torsion, J. Mater. Res. Technol. 24 (2023) 9961–9983.
[16] Buyukozturk, Bakhoum, M.M. Beattie, S.M. Shear behavior of joints in precast concrete segmental bridges. ASCE Journal of Structural Engineering 1990; 116 (12): 3380–3401.
[17] AASHTO. Guide specifications for design and construction of segmental concrete bridges: 2003 interim revisions, 2nd ed; 2003.
[18] X. Zhou, N. Mickleborough, Z. Li, Shear strength of joints in precast concrete segmental bridges, Acids Struct. J. 102 (1) (2005) 3–11.
[19] Concrete Society. Durable post-tensioned concrete structures, Technical Report No. 72. Concrete Society, 2010.
[20] A. Yuan, C. Yang, J. Wang, L. Chen, R. Lu, Shear behavior of epoxy resin joints in precast concrete segmental bridges, J. Bridge Eng. 24 (4) (2019), 04019009.
[21] R.A. Barnes, G.C. Mays, The transfer of stress through a steel to concrete adhesive bond, Int. J. Adhes. Adhes. 21 (2001) 495–502.
[22] Romback, G. Precast segmental box girder bridges with external prestressing-design and construction. INSA Rennes Technical University, Hamburg-Harburg, Germany, 2002.
[23] J.G. Teng, J.F. Chen, S.T. Smith, L. Lam, FRP strengthened RC structures, John Wiley & Sons, U.K, 2002.
[24] D. De Domenico, P. Fuschi, S. Pardo, A.A. Pisano, Strengthening of steel-reinforced concrete structural elements by externally bonded FRP sheets and evaluation of their load carrying capacity, Compos. Struct. 118 (2014) 377–384.
[25] Pellegrino, C. and Sena-Cruz, J. Design procedures for the use of composites in strengthening of reinforced concrete structures: state-of-the-art report of the RILEM Technical Committee 234-DUC, 2016.
[26] D.H. Lee, S.-J. Han, K.S. Kim, J.M. LaFave, Shear strength of reinforced concrete beams strengthened in shear using externally-bonded FRP composites, Compos. Struct. 173 (2017) 177–187.
[27] M. Chellapandian, S.S. Prakash, A. Sharma, Experimental and finite element studies on the flexural behavior of reinforced concrete elements strengthened with hybrid FRP technique, Compos. Struct. 208 (2019) 466–478.
[28] Y. Zhou, J. Zhang, W. Li, B. Hu, X. Huang, Reliability-based design analysis of FRP shear strengthened reinforced concrete beams considering different FRP configurations, Compos. Struct. 237 (2020), 111957.
[29] L.A. Modesti, A.S. de Vargas, E.L. Schneider, Repairing concrete with epoxy adhesives, Int. J. Adhes. Adhes. 101 (2020), 102645.
[30] P. Qiao, Y. Xu, Evaluation of fracture energy of composite-concrete bonded interfaces using three-point bend tests, J. Compos. Constr. 8 (4) (2004) 352–359.
[31] A. Momayez, M.R. Ehsani, A.A. Ramezanianpour, H. Rajaie, Comparison of methods for evaluating bond strength between concrete substrate and repair materials, Cem. Concr. Res. 35 (2005) 748–757.
[32] Coronado, C. Characterization, modeling and size effect of concrete-epoxy interfaces. Ph.D. thesis, The Pennsylvania State University, University Park, PA. 2006.
[33] E.N.B.S. Júlio, P. Santos, D.D. Costa, Modified slant shear test to enforce adhesive failure, Constr. Build. Mater. 41 (2012) 673–680.
[34] M. Newlands, N. Khosravi, R. Jones, L. Chernin, Mechanical performance of statically loaded flat face epoxy bonded concrete joints, Mater. Struct. 51 (49) (2018) 1–14.
[35] G.H. Ahmed, O.Q. Aziz, Shear behavior of dry and epoxied joints in precast concrete segmental box girder bridges under direct shear loading, Eng. Struct. 182 (2019) 89–100.
[36] Correlated Solutions [Online]. Available at: ⟨www.correlatedsolutions.com⟩ [Accessed February 2015].
[37] BSI. BS 8500–2:2015+A1:2016. Concrete – Complementary British Standard to BS EN 206. Part 2: Specification for constituent materials and concrete. London: British Standards Institution, 2015.
[38] BSI. BS 1881–125, Testing concrete, Methods for mixing and sampling fresh concrete in the laboratory. London: British Standards Institution, 2013.
[39] A. Zotti, S. Zuppolini, M. Zarrelli, A. Borriello, Fracture toughening mechanisms in epoxy adhesives. Adhesives-Applications and Properties, InTech,, 2016.
[40] Q. Guo, Thermosets: Structure, properties and applications, Cambridge, UK; Philadelphia. PA, Cambridge, UK; Philadelphia, PA, Woodhead Publishing,, 2012.
[41] ASTM D638, Standard test method for tensile properties of plastics. ASTM International, West Conshohocken, PA, 2014.
[42] BSI. BS EN 1994–1-1 Eurocode 4. Design of composite steel and concrete structures. General rules and rules for buildings. London: British Standards Institution, 2004.
[43] A. Si Larbi, E. Ferrier, B. Jurkiewiez, P. Hamelin, Static behaviour of steel concrete beam connected by bonding, Eng. Struct. 29 (2007) 1034–1042.
[44] ACI-ASCE 445 2013. 445.1R-12, Report on Torsion in Structural Concrete. 92, CI-ASCE Committee, 2013.